IEEE Access
Multidisciplinary | Rapid Review | Open Access Journal

SPECIAL SECTION ON EMERGING TRENDS, ISSUES AND CHALLENGES FOR ARRAY SIGNAL PROCESSING AND ITS APPLICATIONS IN SMART CITY

Received December 9, 2019, accepted January 2, 2020, date of publication January 20, 2020, date of current version January 30, 2020.

Digital Object Identifier 10.1109/ACCESS.2020.2968085

Comparison Between Back Projection Algorithm and Range Migration Algorithm in Terahertz Imaging

GUANWEN WANG[1], FENG QI[1,2,3,4,5], ZHI LIU[6], CUILING LIU[7], CHUNGUI XING[8], AND WEI NING[6]

[1]College of Electronic Information Engineering, Shenyang Aerospace University, Shenyang 110000, China
[2]Shenyang Institute of Automation, Chinese Academy of Sciences, Shenyang 110016, China
[3]Institutes for Robotics and Intelligent Manufacturing, Chinese Academy of Sciences, Shenyang 110016, China
[4]Key Laboratory of Opto-Electronic Information Processing, Chinese Academy of Sciences, Shenyang 110016, China
[5]The Key Lab of Image Understanding and Computer Vision, Shenyang 110016, China
[6]College of Information Science and Engineering, Northeastern University, Shenyang 110169, China
[7]Beijing Key Laboratory of Big Data Technology for Food Safety, Beijing Technology and Business University, Beijing 100048, China
[8]College of Electronic Science and Engineering, Jilin University, Changchun 130012, China

Corresponding authors: Feng Qi (qifeng@sia.cn) and Cuiling Liu (liucl@btbu.edu.cn)

This work was supported in part by the Beijing Key Laboratory of Big Data Technology for Food Safety, Beijing Technology and Business University Inspection of Illegal Cooking-Oil by Using THz Imaging and Spectroscopy Technologies, in part by the Beijing Natural Science Foundation of China under Grant 4182017, in part by the National Key Research and Development Program of China under Grant 2016YFC0102900, and in part by the National Natural Science Foundation of China under Grant 61605235, Grant 61801467, and Grant 61804160.

ABSTRACT Back projection algorithm (BPA) and range migration algorithm (RMA) are two common approaches for image reconstruction in synthetic aperture radar (SAR) imaging. Imaging is implemented in spatial domain and spatial frequency domain, respectively and these two methods are often considered to generate the same results. This is true in normal microwave/millimeter wave SAR imaging systems, since the object of interests is located far away and the applied wavelength is long. In this case, the location of the object is the most important issue and there is no impetus to image the object with very fine details. In case of terahertz (THz) imaging, we have found some differences by using the two algorithms above, including the position of the object and resolution in 2D and 3D imaging. Some insights are given and we believe there should be some guidelines regarding the pros and cons before choosing the exact algorithm, especially when high-performance imaging is pursued.

INDEX TERMS Ambient environment sensing, THz imaging, image reconstruction.

I. INTRODUCTION

Autonomous driving is important for smart traffic in future, which requires accurate positioning and imaging abilities [1]. Based on visible light or near-infrared facilities, Lidar and cameras are being investigated intensively. Such facilities are welcome since they deliver images similar to what we can see by eyes. However, since these systems relies on optics, they do not perform well in bad-weather conditions like fog, rain and snow. All-weather sensing ability is expected consequently. Positioning systems are possible at radio frequencies, but they do not supply images and accuracy is limited due to the long wavelengths. Millimeter wave radars are popular nowadays and they have already worked well for anti-collision and blind-zone detection. However, they do not offer imaging ability nowadays. It is expected that high-performance imaging is desired in future [2], which is able to supply people with decent pictures of static environment in bad weather. A THz imager might be a good candidate for such applications in future due to the fine resolution. Moreover, they will not be influenced by weather.

Due to the progress in fabrication, material science, communication and laser technologies, THz technology developed rapidly in the past ten years [3]–[9]. For THz imaging, there are two common working mechanisms which are focal plane imaging and SAR imaging, respectively. For the first one, an object can be illustrated well by measuring the intensity distribution on imaging plane; while for the

The associate editor coordinating the review of this manuscript and approving it for publication was Liangtian Wan.

latter one, coherent measurements should be implemented on a dedicated aperture and the object is focused via signal processing by making the wave propagates backwards to its exact location. In case of SAR imaging, there are two popular algorithms for digital focusing process, including back projection algorithm (BPA) and range migration algorithm (RMA), which implement the calculations in spatial domain and spatial frequency domain, respectively. Limited by the power of THz transmitters and the sensitivity of detectors nowadays, near-field imaging dominates and far-field imaging is rare. Objects can be imaged with very fine details thanks to the short wavelengths at THz frequencies. However, THz imaging technique is not as mature as classical microwave imaging. Whether we should simply copy previous success at microwave frequencies is a question and the near-field scenario can make some difference.

BPA was first proposed in 1991 and it was applied to the airborne radar for remote sensing. After collecting echoes, both the geography and objects on the ground can be reconstructed [10]. The complexity of this algorithm is $O(N^3)$, with N as the number of transmitting pulses and the N by N to discretize the measured area. It may cause a problem for real-time imaging due to the huge calculation amount. With the aid of fast Fourier transform (FFT), the complexity changes from $O(N^3)$ to $O(N^2 \log N)$ [11]. Range migration algorithm (RMA) was first proposed in 1987 [12]. It has the complexity of $O(N^2 \log N)$, which is comparable to the fast BPA in [11]. It has been applied effectively in a lot of scenarios, including seismic survey [13], security checking [14], 3D reconstruction [15], biological applications [16] and so on.

These two algorithms have the same function and they are just implemented in two different domains. There are few reports on the comparison of them at microwave frequencies. In [17], simulation studies have been done at 400 MHz and the target is 1025 meters' away. It is concluded that these two algorithms have almost the same performance, with BPA taking more time on calculations. In [18], comparisons are implemented based on the measurements of a UWB system with the central frequency at 225MHz and it is concluded that the two algorithms have the same range resolution. In [19], RMA has better performance in cross range resolution and it has lower side lobe levels than the BPA for the point spread function. By sweeping the frequency from 90 GHz to 95 GHz, RMA gives the cross range resolution of 1.22 cm, which is slightly better than 1.4 cm of BPA. While, for range resolution, BPA is 3.31cm and RMA is 3.35cm. However, due to the low frequencies, such differences are not clear, and there is a lack of insights. Moreover, to the best of our knowledge, there is no comparison between these methods for THz imaging.

In this paper, BPA and RMA in THz near-field imaging, are compared. According to the experimental results, there are some obvious differences. We will try to explain the phenomenon and pros and cons for both algorithms are given. This paper is structured as followčžIn section two, a brief review of the two algorithms is implemented. In section three, experimental studies are reported in both 2D and 3D imaging scenarios. Section four gives conclusion of this paper.

II. REVIEW OF ALGORITHMS

A. BRIEF REVIEW OF BPA

For a SAR imaging system, the transmitted signal can be defined as

$$s(t) = \mathrm{A}e^{j2\pi ft} \tag{1}$$

where A is the amplitude of signal, j is a unit of complex number, f is the frequency of transmitted signal. The back-scattered wave of the target is

$$s(m, f) = \delta_m s(t) e^{j2\pi f \tau_m} \tag{2}$$

where m represents the position of receiving antenna during scanning process, τ is twice the time delay of signal from the antenna to the object. Time delay τ is defined as

$$\tau = \frac{2d}{c} \tag{3}$$

where d is the distance between the antenna and the target, c is the speed of light. The main process of BPA can be expressed as

$$\delta_{BP}(x, y, z) = \sum_{m=1}^{M} \sum_{n=1}^{N} \mathrm{s}(m, f_n) e^{-j4\pi f_n d_m / c} \tag{4}$$

where M is the number of scanning points. According to equation (4), the object function can be calculated according to the complex ratio between transmitting and receiving signals by solving the matrix for a given distance. By integrating echoes at different frequencies, BPA can reconstruct the object.

B. BRIEF REVIEW OF RMA

RMA is also called the ω-k algorithm. Through back propagation of electromagnetic wave, digital focusing can be realized via signal processing [20]. Since the wave travels a round-trip,

$$k_x^2 + k_y^2 + k_z^2 = (2k)^2 \tag{5}$$

where $k = \omega/c$ is the wavenumber and $\omega = 2\pi f$ is the angular frequency. k_x, k_y, k_z indicate three components of k along the x, y, z-*axis*, with

$$k_z = \sqrt{4\left(\frac{\omega}{c}\right)^2 - k_x^2 - k_y^2} \tag{6}$$

Reflection coefficient is expressed as

$$\begin{aligned} &\delta(x, y, z) \\ &\quad = IFT_{3D}[Stolt[FT_{2D}[s'(x, y, \omega)]e^{-jk_z z}]] \\ &\quad = IFT_{3D}[Stolt[FT_{2D}[s'(x, y, \omega)]e^{-j\sqrt{4k^2 - k_x^2 - k_y^2}\, z}]] \end{aligned} \tag{7}$$

where *Stolt*[ ] is Stolt interpolation for a function [21], which deals with the uneven distribution of wavenumbers in spatial frequency domain for ease of numerical calculations.

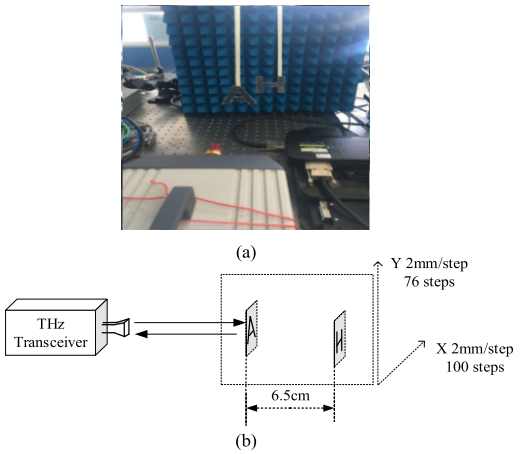

FIGURE 1. Experimental setup for THz near-field SAR imaging. a) Photo of the measurement setup. b) Sketch map of the experiments.

III. EXPERIMENTAL STUDIES

A. EXPERIMENTAL SETUP

The facilities and object of interests are illustrated in Figure 1. The two letters of *A* and *H* are made up of metal foil and the interval between them is 6.5 cm. Frequency sweeping is done between 270 GHz to 290 GHz for data acquisition, with a scanning area of 15 cm × 20 cm.

Figure 2 illustrates the raw data of measurements, and the letters of *A* and *H* are not clear due to diffraction. The edges of the letters are blurred. Moreover, the contrast ratio between background and the target is low. In order to visualize the letters clearly, two imaging algorithms are applied to reconstruct the objects.

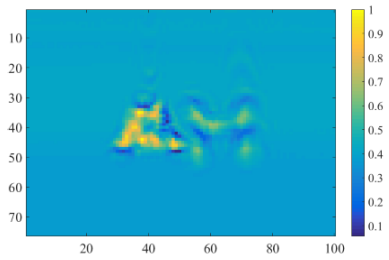

FIGURE 2. 2-D illustration of the raw data.

B. COMPARISONS OF 2-D IMAGING

By using BPA and RMA, restored images are shown in Figure 3, which are much more clear than in Figure 2. Although both algorithms can recover the letters, RMA performs better than BPA. This is especially true at the edge of the letters. Moreover, two bars made of High Density Polyethylene(HDPE) are applied to fix the letters, which are quite visible in Figure 3 (c) and Figure 3 (d). In Figure 3 (a), an *H* is quite visible besides the letter *A*, although we only wish to see the letter *A* in this plane. In Figure 3 (c), the letter *H* is more blurred than in Figure 3 (a). It means that RMA has better filtering performance for the out-of-focus objects.

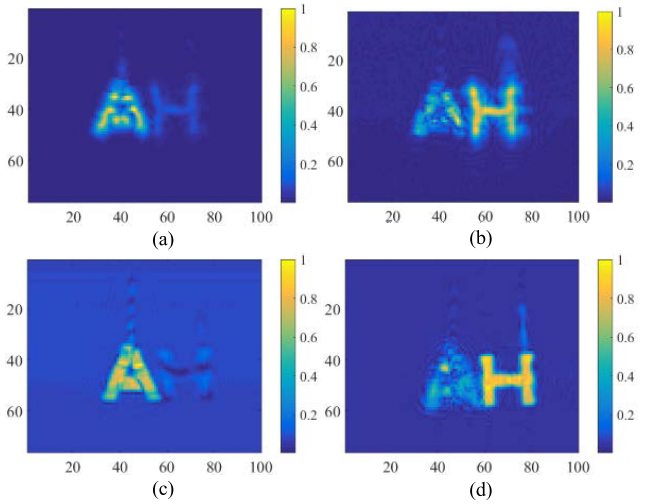

FIGURE 3. 2-D imaging result by BPA and RMA. a) Letter 'A' by BPA. b) Letter 'H' by BPA. c) Letter 'A' by RMA. d) Letter 'H' by RMA.

While in BPA, it is easier to sense those objects in front of or behind the focal plane, implying that it has a larger equivalent depth of focus.

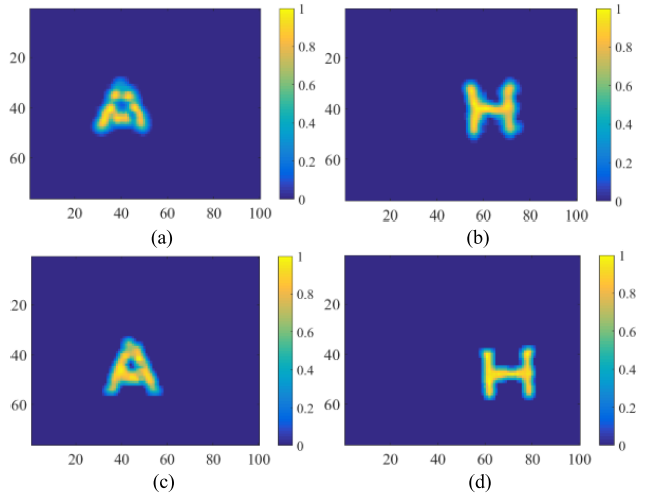

FIGURE 4. 2-D imaging after threshold processing and mean filtering. a) Letter 'A' by BPA. b) Letter 'H' by BPA. c) Letter 'A' by RMA. d) Letter 'H' by RMA.

To visualize the result more clearly, threshold processing and averaging operations are implemented with corresponding results shown in Figure 3. Consequently, the contour of the target is more clear, and the noise of the target-free area is suppressed well in Figure 4. Obviously, there is a clear offset for the letter *H*. By using BPA and RMA, the letter is not in the same position. Since BPA only performs optical path calibration for echoes at each frequency, the position of the object should be accurate. However, by using RMA, Stolt interpolation and approximations are implemented so as to calculate the Fourier transform numerically. These could make the calculations different besides a pure transform

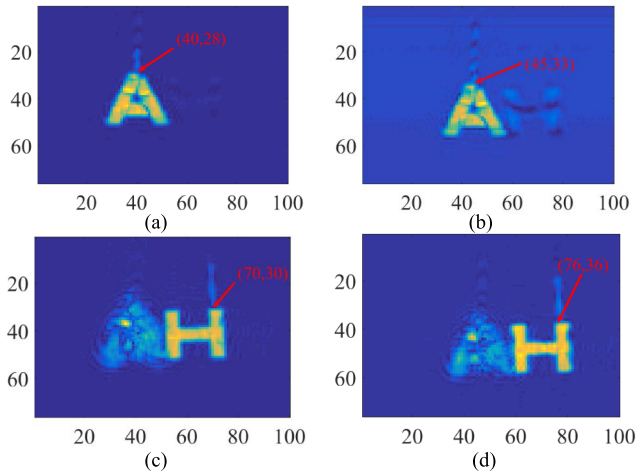

FIGURE 5. 2-D imaging by RMA. (a) (c) Without Stolt interpolation. (b) (d) After Stolt interpolation.

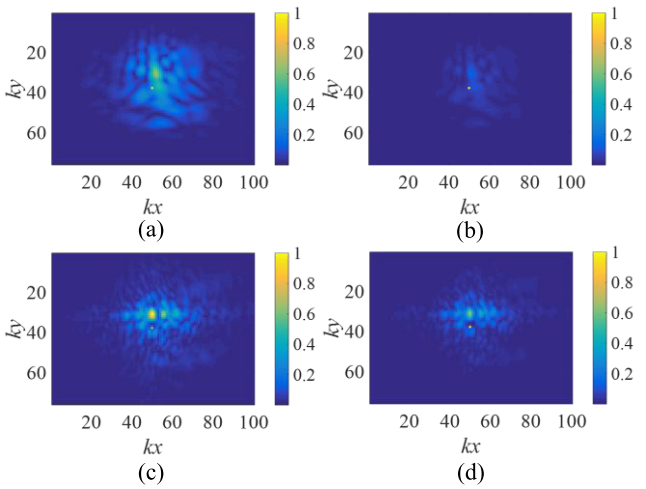

FIGURE 6. Wavenumber domain 2D data. a) Letter *A* without Stolt interpolation. b) Letter *A* after Stolt interpolation. c) Letter *H* without Stolt interpolation. d) Letter *H* after Stolt interpolation.

in mathematics. Consequently, the object moves away from its exact location, which is a cost for the processing above.

According to Figure 4, there is an offset for the letter *H*. Since BPA works in spatial domain, the location of the object should be accurate. While for RMA, Stolt interpolation is applied for ease of numerical calculations. This might change the calculation results. To understand the influence of Stolt interpolation in 2D imaging, the following two cases have been compared: first, each letter is fixed at its exact location and 2D RMA is implemented at a single frequency; then as above, Stolt interpolation is application and 3D IFFT is applied to reconstruct the letter without knowing the distance. In this way, the only reason for the differences in images are due to the Stolt interpolation solely.

In Figure 5, imaging results with and without Stolt interpolation are compared. Obviously, 2D RMA operations without Stolt interpolation give higher resolution. Besides the letter *A*, there is a blurred letter *H* in Figure 5 (b). As shown in Figure 5 (c) and Figure 5 (d), the letter *A* in front of the letter *H* can be visualized somewhat. The Stolt interpolation degrades the imaging performance, and the object is not at the perfect location in 3D reconstruction. While by giving the exact distance of the object, it is possible to give a better focusing effect. Moreover, there a clear offset in both letters. The letter *A* shifts 5 pixels and the letter *H* shifts 6 pixels in Figure 5. For imaging applications, it might not be a trouble. However, in case of positioning operations, Stolt interpolation may introduce errors in this way.

Similar comparisons have also been implemented in spatial frequency domain, with the results shown in Figure 6. The left two figures give the accurate results; while the right two figures correspond to the results by using Stolt interpolation. It is obviously that spectrums with and without interpolation are similar in shape, but after using Stolt interpolation, some high spatial components are lost, which account for the resolution in imaging. Moreover, DC power is lower in Figure 6 (b) and (d), which decrease the contrast in reconstructed image. To make the comparisons quantitatively, correlation has been calculated, which can describe the similarity of the figures mathematically.

Perform correlation calculation on the data before and after Stolt interpolation in Figure 5 and Figure 6, respectively. In Figure 5, the correlations of (a)(b) and (c)(d) are 0.465 and 0.240. The results show that both coordinates *A* and *H* produce coordinate offsets, and the offset of *H* is larger than *A*. The correlation calculation is performed only on the matrix of the letter corresponding size. The correlations of the letters *A* and *H* before and after the Stolt interpolation are 0.739 and 0.884, respectively. By removing the effect of coordinate offset on correlation, the correlations of letter *A* and *H* before and after Stolt interpolation have a significant improvement. It also can be found that after removing the influence of coordinate offset, letter *H* has better correlation than *A*. It means that in addition to shifting the letters, interpolation also introduces background noise. Making calculation in Figure 6, the correlations of (a)(b) and (c)(d) are 0.898 and 0.971. When considering the relationship between individual pixels and coordinates, the correlation of *H* is lower, which means that *H* has more offsets. When only the letter edge and energy distribution are considered, *H* has higher correlation. This is the same as the correlation of the wavenumber domain.

C. COMPARISON OF 3-D IMAGING

Thanks to the large bandwidth of the THz systems, 3D imaging is feasible with a fine range resolution. To visualize the results more clearly, point cloud processing is performed. Each point corresponds to the maxima in terms of amplitude along the *z*-axis. Threshold processing is implemented also, in order to remove the background noise outside the target. By doing the operations above, 3D figures are obtained. Generally, range resolution of a SAR imaging system is decided

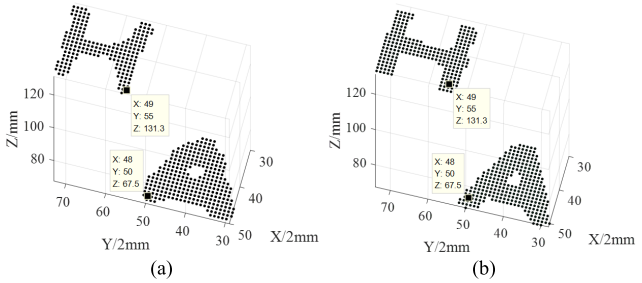

FIGURE 7. 3-D imaging of target with point cloud map. a) by using BPA. b) by using RMA.

by the bandwidth of the transceiver, which is

$$\Delta z = c/2B \tag{8}$$

where B is the applied bandwidth. Thus, the range resolution corresponding to the 20 GHz bandwidth is 7.5 mm. According to Figure 1(b), the distance between the letters A and H is 65mm. Figure 7 (a) corresponds to the 3D image by using BPA, while Figure 7 (b) is 3D image obtained by using RMA. According to Figure 4, the calculated distance between A and H is 63.75 mm by BPA, and 60 mm by RMA. Thus the range calculation errors of BPA and RMA are 1.25mm and 5mm. Contrary to 2D imaging, BPA has a better range resolution.

In order to compare the imaging effects of these two algorithms further, a metal ladder with the step of 1 mm is imaged between 220 GHz and 325 GHz. The theoretical range resolution is 1.428 mm corresponding to the bandwidth of 105 GHz. Thus the step of metal ladder is smaller than the theoretical limit. The model of target is shown in Figure 8.

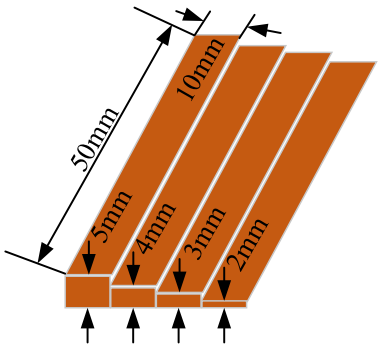

FIGURE 8. Model of the applied ladder.

In Figure 9, it can be seen that BPA performs better in visualizing each step of the ladder than RMA. Corresponding to the profile of BPA, four steps of ladder are distinguished clearly. RMA can only distinguish each two steps, with the distance of 2 mm. BPA does not make any approximation in range direction and it is calculated directly.

Although both algorithms can give good images, it is important to know the advantages and disadvantages. Although BPA can be more accurate in terms of range

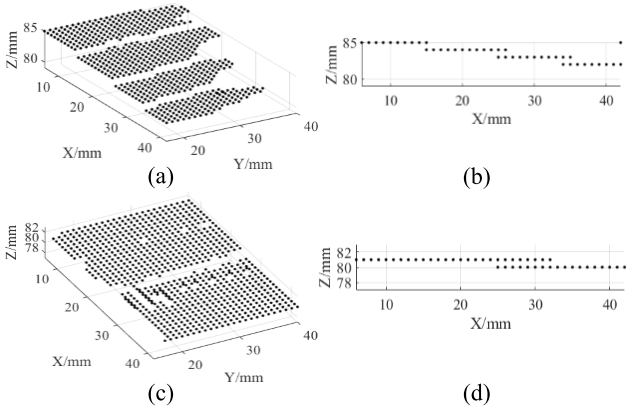

FIGURE 9. 3-D imaging of ladder with point cloud map. a) BPA. b) RMA.

resolution, it is more calculation intensive and it might be not suitable for real-time applications. For 3D imaging of static scenarios or absolute measurements, it might be more suitable. RMA can be faster and it is much more efficient for 2D imaging. For future applications in smart cities, THz imagers might be promising regarding its all-weather operation ability and decent imaging performance. Which algorithm to choose depends on exact applications and both accuracy and calculation speed need to be improved in future, accompanied with hardware implementation.

IV. CONCLUSION

In this paper, terahertz SAR imaging algorithms are investigated. For 2D imaging, RMA performs better in cross resolution, but there might be offset effect due to Stolt interpolation. For 3D imaging, BPA performs overcomes RMA since it implements the calculations in spatial domain directly and there are no interpolation and FFT operations, which may generate numerical errors in practice. BPA may break the limit for range resolution defined by the Fourier transform, which is the case in RMA. In practice, which algorithm to choose depends on actual requirements for a dedicated scenario and various factors should be considered carefully including the accuracy of positioning/imaging and the calculation speed.

REFERENCES

[1] H. Wang, L. Wan, M. Dong, K. Ota, and X. Wang, "Assistant vehicle localization based on three collaborative base stations via SBL-based robust DOA estimation," *IEEE Internet Things J.*, vol. 6, no. 3, pp. 5766–5777, Jun. 2019.

[2] F. Wen, Z. Zhang, and G. Zhang, "Joint DOD and DOA estimation for bistatic MIMO radar: A covariance trilinear decomposition perspective," *IEEE Access*, vol. 7, pp. 53273–53283, 2019.

[3] X. Wang, L. Wan, M. Huang, C. Shen, and K. Zhang, "Polarization channel estimation for circular and non-circular signals in massive MIMO systems," *IEEE J. Sel. Topics Signal Process.*, vol. 13, no. 5, pp. 1001–1016, Sep. 2019.

[4] S. K. Goudos, M. Deruyck, D. Plets, L. Martens, K. E. Psannis, P. Sarigiannidis, and W. Joseph, "A novel design approach for 5G massive MIMO and NB-IoT green networks using a hybrid Jaya-differential evolution algorithm," *IEEE Access*, vol. 7, pp. 105687–105700, 2019.

[5] S. Kutia, S. H. Chauhdary, C. Iwendi, L. Liu, W. Yong, and A. K. Bashir, "Socio-technological factors affecting user–adoption of eHealth functionalities: A case study of China and Ukraine eHealth systems," *IEEE Access*, vol. 7, pp. 90777–90788, 2019.
[6] T. P. Raptis, A. Passarella, and M. Conti, "Data management in industry 4.0: State of the art and open challenges," *IEEE Access*, vol. 7, pp. 97052–97093, 2019.
[7] K. Cooper, R. Dengler, N. Llombart, T. Bryllert, G. Chattopadhyay, E. Schlecht, J. Gill, C. Lee, A. Skalare, I. Mehdi, and P. Siegel, "Penetrating 3-D imaging at 4- and 25-m range using a submillimeter-wave radar," *IEEE Trans. Microw. Theory Techn.*, vol. 56, no. 12, pp. 2771–2778, Dec. 2008.
[8] H. Balacey, B. Recur, J.-B. Perraud, J. B. Sleiman, J.-P. Guillet, and P. Mounaix, "Advanced processing sequence for 3-D THz imaging," *IEEE Trans. THz Sci. Technol.*, vol. 6, no. 2, pp. 191–198, Mar. 2016.
[9] T. S. Rappaport, Y. Xing, O. Kanhere, S. Ju, A. Madanayake, S. Mandal, A. Alkhateeb, and G. C. Trichopoulos, "Wireless communications and applications above 100 GHz: Opportunities and challenges for 6G and beyond," *IEEE Access*, vol. 7, pp. 78729–78757, 2019.
[10] J. W. Mccorkle, "Focusing of synthetic aperture ultra wideband data," in *Proc. IEEE Int. Conf. Syst. Eng.*, Aug. 1991, pp. 1–5.
[11] A. Gaibel and A. Boag, "Back-projection SAR imaging using FFT," in *Proc. Eur. Radar Conf.*, Oct. 2016, pp. 69–72.
[12] F. Rocca, C. Cafforio, and C. Prati, "Synthetic aperture radar: A new application for wave equation techniques," *Geophys. Prospecting*, vol. 37, no. 7, pp. 809–830, 2006.
[13] C. Cafforio, C. Prati, and F. Rocca, "SAR data focusing using seismic migration techniques," *IEEE Trans. Aerosp. Electron. Syst.*, vol. 27, no. 2, pp. 194–207, Mar. 1991.
[14] D. Sheen, D. Mcmakin, and T. Hall, "Three-dimensional millimeter-wave imaging for concealed weapon detection," *IEEE Trans. Microw. Theory Techn.*, vol. 49, no. 9, pp. 1581–1592, Sep. 2001.
[15] J. Lopez-Sahcnez and J. Fortuny-Guasch, "3-D radar imaging using range migration techniques," *IEEE Trans. Antennas Propag.*, vol. 48, no. 5, pp. 728–737, May 2000.
[16] N. V. Petrov, A. A. Gorodetsky, and V. G. Bespalov, "Holography and phase retrieval in terahertz imaging," *Proc. SPIE*, vol. 8846, Sep. 2013, Art. no. 88460S.
[17] Y. H. Z. Guofu, "A comparison of back-projection and range migration UWB-SAR focusing algorithms," *Electron. Technol.*, pp. 53–55, 2008.
[18] Y. Na, Y. Lu, and H. Sun, "A comparison of back-projection and range migration algorithms for ultra-wideband SAR imaging," in *Proc. IEEE Workshop Sensor Array Multichannel Signal Process.*, Sep. 2006, pp. 320–324
[19] E. Yigit, "Short-range ground-based synthetic aperture radar imaging: Performance comparison between frequency-wavenumber migration and back-projection algorithms," *J. Appl. Remote Sens*, vol. 7, no. 1, Nov. 2013, Art. no. 073483.
[20] D. Loewenthal, L. Lu, R. Roberson, and J. Sherwood, "The wave equation applied to migration," *Geophys. Prospecting*, vol. 24, no. 2, pp. 380–399, Jun. 1976.
[21] R. H. Stolt, "Migration by fourier transform," *Geophysics*, vol. 43, no. 1, pp. 23–48, Feb. 1978.

GUANWEN WANG received the B.Sc. degree from Anshan Normal University, in 2017, and the M.Sc. degree from Shenyang Aerospace University, in 2019. He will pursue the Ph.D. degree with the Shenyang Institute of Automation, Chinese Academy of Sciences, in September 2020. His research interests include radar imaging and THz imaging algorithms.

FENG QI received the B.Sc. degree from Zhejiang University and the M.Sc. and Ph.D. degrees from Katholieke Universiteit Leuven, Belgium, in 2005 and 2011, respectively. Since 2005, he has been involved in antennas and millimeter wave imaging. Then, he joined RIKEN, Japan. He did research on THz radar in nonlinear optics with Goethe University Frankfurt, Germany, and the University of Birmingham, U.K. In 2015, he joined as a Professor with the THz Imaging Laboratory, Shenyang Institute of Automation, Chinese Academy of Sciences. He is also a Supervisor with Shenyang Aerospace University. His current research interests include microwaves, lasers, and radars. Since 2012, he has been a TPC Member of the Global Symposium on Millimeter Waves. He has received the Best Paper Award, in 2014.

ZHI LIU is currently pursuing the degree in information science and engineering with Northeastern University. He is also doing an internship with the THz Imaging Laboratory, Shenyang Institute of Automation, Chinese Academy of Sciences. His research interest is THz imaging.

CUILING LIU received the Ph.D. degree from the Harbin Institute of Technology University, in 2002. She is currently a Professor with the School of Computer and Information Engineering, Beijing Technology and Business University, and the first-level Discipline Leader in control science and engineering. Her current research interests include food safety testing technology and data processing, system modeling, and simulation.

CHUNGUI XING received the B.Sc. and M.Sc. degrees from the Dalian University of Technology, in 2001 and 2004, respectively. He is currently pursuing the Ph.D. degree with the College of Electronic Science and Engineering, Jilin University. His research interests include THz imaging and compressed sensing.

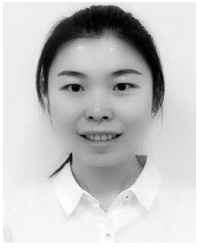

WEI NING received the B.Sc. degree from Northeastern University, in 2009, and the M.Sc. degree from the North China University of Technology, in 2013. She is currently pursuing the Ph.D. degree with the School of Computer Science and Engineering, Northeastern University. Her research interests include THz imaging and THz image processing.